Regulation of CNS synapses by neuronal MHC class I

C. Alex Goddard*, Daniel A. Butts†, and Carla J. Shatz‡

Department of Neurobiology, Harvard Medical School, Boston, MA 02115

Contributed by Carla J. Shatz, March 6, 2007 (sent for review January 9, 2007)

Until recently, neurons in the healthy brain were considered immune-privileged because they did not appear to express MHC class I (MHCI). However, MHCI mRNA was found to be regulated by neural activity in the developing visual system and has been detected in other regions of the uninjured brain. Here we show that MHCI regulates aspects of synaptic function in response to activity. MHCI protein is colocalized postsynaptically with PSD-95 in dendrites of hippocampal neurons. *In vitro*, whole-cell recordings of hippocampal neurons from β2m/TAP1 knockout (KO) mice, which have reduced MHCI surface levels, indicate a 40% increase in mini-EPSC (mEPSC) frequency. mEPSC frequency is also increased 100% in layer 4 cortical neurons. Similarly, in KO hippocampal cultures, there is a modest increase in the size of presynaptic boutons relative to WT, whereas postsynaptic parameters (PSD-95 puncta size and mEPSC amplitude) are normal. In EM of intact hippocampus, KO synapses show a corresponding increase in vesicles number. Finally, KO neurons *in vitro* fail to respond normally to TTX treatment by scaling up synaptic parameters. Together, these results suggest that postsynaptically localized MHCI acts in homeostatic regulation of synaptic function and morphology during development and in response to activity blockade. The results also imply that MHCI acts retrogradely across the synapse to translate activity into lasting change in structure.

homeostatic | neuron | plasticity | synapsin | PSD-95

Experience transduced into neural activity is required for proper brain development (1). The process by which neural activity remodels synaptic connections during development is termed "activity-dependent plasticity," in which electrical signals induce specific patterns of gene transcription to alter synaptic properties and structural connectivity. Genes including BDNF and CamKII are known to be critical for this plasticity (2–4); however, many other molecules are likely involved as well.

MHC class I (MHCI) family members are well known for their roles in cellular immunity, but a neuronal function has not been generally appreciated. In the immune system, MHCI genes act in concert with T cell receptors to discriminate self- versus non-self-proteins. The CNS was considered "immune privileged," in part, because it was thought that healthy neurons do not express MHCI protein (5, 6). Recently, MHCI gene family members have been found at low levels in CNS neurons (7–11). MHCI mRNA is expressed and regulated in cortical and thalamic neurons during development and is down-regulated by chronic activity blockade with Tetrodotoxin (TTX) *in vivo* (7). MHCI is also a downstream target of the transcription factor CREB, required for Hebbian synaptic plasticity (8, 12, 13). MHCI is thus implicated in several forms of activity-dependent synaptic plasticity.

The MHCI gene family includes >70 members in rodents (14). The proteins encoded are heavy chains comprising the largest portion of the MHCI protein complex. Functional MHCI is usually a trimer consisting of the heavy chain, β-2-microglobulin (β2m), and a 9–11 aa peptide generated from proteosomal degradation (15). The transporter associated with antigen processing [(TAP) a heterodimer of TAP1 and TAP2] is required for transport of peptide fragments from cytoplasm into the lumen of the endoplasmic reticulum for assembly (16). For most MHCI proteins, cell surface expression of heavy chain only occurs if β2m and peptide are present (16, 17). In their absence, both surface and intracellular levels of MHCI are down-regulated (18). Therefore, brains of mice deficient in β2m and TAP1 were studied here as MHCI "loss of function." These mice have altered Hebbian synaptic plasticity in the hippocampus and abnormal patterning of visual system connections (19), reminiscent of animals that have undergone blockade of neural activity (20–22). Despite this new appreciation of MHCI function in neuronal plasticity and the discovery of a candidate neuronal receptor (23, 24), however, it is not known whether MHCI protein is present at CNS synapses or whether it is part of molecular machinery regulating synaptic function and structure.

Here we investigate the subcellular localization of MHCI and show that neurons with low levels of MHCI have altered synaptic function and structure. Moreover, MHCI appears to play a role in homeostatically regulating aspects of synaptic structure and function in response to low levels of neural activity.

Results

The subcellular localization of MHCI protein was examined by immunostaining cultures of hippocampal neurons with a pan-specific MHCI antibody, Ox18 (7, 25). Punctate immunostaining is present in soma and dendrites (Fig. 1*a*); at higher magnification, MHCI immunostaining is in spine-like dendritic protuberances (Fig. 1*b*). To determine prior postsynaptic location for MHCI, PSD-95 [present at postsynaptic densities of excitatory synapses (26)] or synapsin [associated with presynaptic vesicles (27)] was also detected immunofluorescently (Fig. 1*b*). Signal for MHCI protein overlaps extensively with PSD-95 signal; 57% of Ox18 immunoreactive pixels overlap with PSD-95 pixels (Fig. 1*c*). In contrast, the distribution of synapsin immunoreactivity is one of close apposition and minimal overlap with MHCI (Fig. 1 *b* and *c*), suggesting that the two proteins are in separate, adjacent pre- and postsynaptic compartments. Thus, MHCI appears to be located postsynaptically at excitatory synapses, consistent with a recent report of dendritic localization of MHCI mRNAs in hippocampal neurons (28).

Given the presence of MHCI at synapses, as well as previously reported alterations in activity-dependent plasticity in β2m/TAP1 knockout (KO) mice (19), it is possible that cultured KO neurons have altered basal synaptic transmission. Spontaneous mini-EPSCs (mEPSCs) from WT or KO hippocampal cultures were recorded by using whole-cell patch-clamp (Fig. 2*a*). mEPSCs from WT neurons have a median instantaneous frequency of 1.8 Hz and a median amplitude of 7.1 pA. In contrast, the instantaneous frequency of KO mEPSCs is increased 40% (to 2.5

Author contributions: C.A.G., D.A.B., and C.J.S. designed research; C.A.G. performed research; C.A.G. and D.A.B. contributed new reagents/analytic tools; C.A.G. analyzed data; and C.A.G. and C.J.S. wrote the paper.

The authors declare no conflict of interest.

Abbreviations: KO, knockout; MHCI, MHC class I; PSD, postsynaptic densities.

*Present address: Department of Neurobiology, Stanford University, Stanford, CA 94305.

†Present address: Department of Physiology and Biophysics, Institute of Computational Biomedicine, Weill Medical College of Cornell University, New York, NY 10021.

‡To whom correspondence should be addressed. E-mail: carla_shatz@hms.harvard.edu.

This article contains supporting information online at www.pnas.org/cgi/content/full/0702023104/DC1.

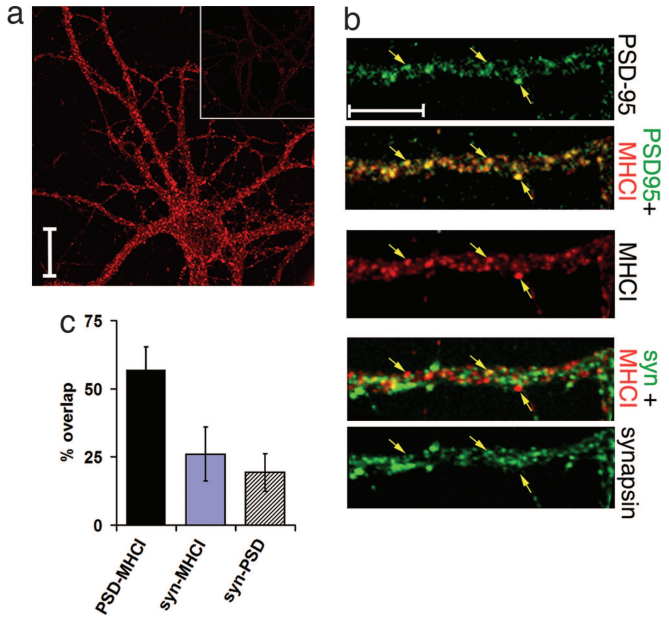

Fig. 1. MHCI is expressed at or near synaptic sites. (*a*) MHCI expression in hippocampal neurons (2 weeks *in vitro*) detected with Ox18 compared with equimolar amount of control mouse IgG (*Inset*). Immunoreactivity is present in soma and dendrites. (Scale bar: 20 μm.) (*b*) High-magnification views of MHCI and synaptic protein immunoreactivity. Antisynapsin antibodies were detected with Cy-2 linked secondary, anti-MHCI with Cy3, and anti-PSD-95 with Cy5. Synaptic proteins are pseudocolored green for comparison with MHCI (red). (*Top*) PSD-95 immunostained puncta marked by arrows; merged PSD-95 and MHCI signals, with nearly complete colocalization. (*Middle*) MHCI immunostaining of dendrites and spines. (*Bottom*) Synapsin immunostaining apposes but does not overlap MHCI immunostaining. (Scale bar: 10 μm.) (*c*) Quantification of the percentage overlap of MHCI immunostaining (Ox18 antibody) with PSD-95 or synapsin (syn); 57.0 $\pm$ 8.4% of MHCI immunoreactive pixels overlap with PSD-95 pixels. However, only 26.1 $\pm$ 9.8% MHCI pixels overlap with synapsin pixels. Synapsin–MHCI overlap vs. PSD-95–MHCI overlap is statistically significant ($P < 0.001$, *t* test). Overlap between synapsin and PSD-95, 19.3 $\pm$ 6.9%. The amount of overlap between synapsin–MHCI vs. synapsin–PSD-95 was not significantly different ($P = 0.2$, *t* test) ($n = 7$ fields of 325 $\times$ 325 μm at 512 $\times$ 512 pixel resolution).

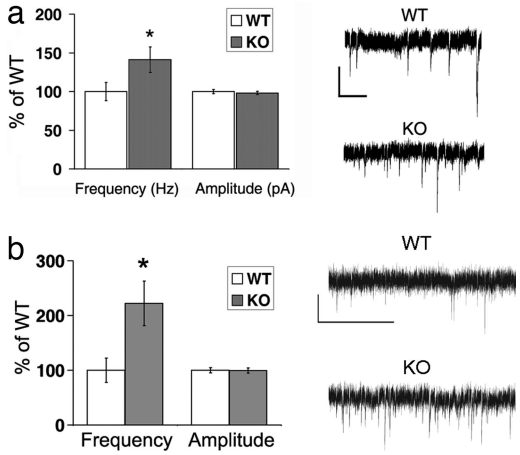

Fig. 2. Basal synaptic function is altered in β2m/TAP1 KO neurons. (*a*) Whole-cell recordings from hippocampal neurons in culture. (*Left*) Frequency of mEPSCs recorded in the basal state from KO (2.5 Hz, $n = 17$ neurons) is greater than that of WT (1.8 Hz, $P < 0.001$, $n = 22$ neurons), but amplitudes do not differ (WT, 7.1; KO, 7.0; $P = 0.98$). Data presented as ratio of KO/WT median instantaneous frequency (1 per interevent interval) or median amplitude. *, significance as calculated by Kolmogorov–Smirnov test of cumulative distribution of events (see Fig. 5 *a* and *b*). (*Right*) Representative traces of mEPSC recordings from WT or KO neurons (2.5 weeks *in vitro*). (Scale bar: 10 pA; 400 msec.) (*b*) Whole-cell recordings from layer 4 neurons in visual cortical slices. (*Left*) mEPSCs from KO are more frequent than WT (WT, $n = 10$ neurons from three animals; KO, $n = 10$ neurons from three animals). Frequency (in Hz) (WT, 2.4 $\pm$ 1.7; KO, 5.3 $\pm$ 3.1; $P = 0.02$). Amplitude (in pA) (WT, 10.8 $\pm$ 1.6; KO, 10.7 $\pm$ 1.6; $P = 0.92$). *, significance by *t* test. (*Right*) Representative traces of mEPSC recordings from WT or KO neurons. (Scale bar: 10 pA; 400 msec.)

Hz). However, mEPSC median amplitude is similar at KO and WT synapses (Fig. 2*a*). These results imply that there is an abnormality in basal synaptic transmission in KO neurons.

MHCI mRNA is observed in many brain regions, including visual cortical neurons (11, 19, 29). To assess whether spontaneous release is abnormal elsewhere in CNS and in a more intact preparation, mEPSCs were recorded from layer 4 neurons in acute slices of visual cortex (Fig. 2*b*) at postnatal days 19–21. The frequency of mEPSCs recorded from KO cortical neurons is 100% greater than that from WT neurons, reminiscent of the hippocampal cultures. As in cultures, mEPSC amplitude is similar in WT and KO. These findings suggest that alterations in basal synaptic transmission occur across various brain regions in mice lacking stable cell surface expression of MHCI.

The increase in mEPSC frequency in KO hippocampal cultures and cortical slices suggests that synaptic organization may also be altered. An increase in mEPSC frequency could be due to an increase in the number or density of synapses (30) or to an increase in probability of release (31, 32). We therefore examined the structural organization of synapses in KO hippocampal cultures. First, we verified that MHCI protein levels are reduced in KO neurons by immunostaining hippocampal cultures with Ox18 (Fig. 3*a*). Consistent with many previous studies of non-neuronal cell types, KO neurons have low levels of MHCI (16, 33).

WT and KO hippocampal cultures were then immunostained for synapsin I to examine presynaptic terminals. There is a modest increase in size of synapsin-immunoreactive boutons in KO cultures: They are ≈6% larger than WT ($P = 0.03$) (Fig. 3). Furthermore, boutons immunostained for vGluT1 and vGluT2, two isoforms of the excitatory, presynaptically localized vesicular glutamate transporter (34, 35), are also roughly 6% larger in KO ($P = 0.02$) (Fig. 3 *b* and *c*). Together these observations suggest a general alteration in excitatory presynaptic boutons, rather than a change specific to either protein alone.

Postsynaptic organization of WT and KO neurons was assessed by immunostaining for PSD-95, known to correlate with AMPA receptor levels in spines (30, 36, 37). Unlike the observed presynaptic changes, PSD-95 immunostained puncta in KO neurons are not significantly different in size from WT (Fig. 3 *b* and *c*), nor did synaptic density differ between WT and KO [supporting information (SI) Fig. 6]. Thus, it appears that diminished postsynaptic levels of MHCI protein are associated with a modest enlargement of presynaptic boutons. The significant increase in mEPSC frequency is probably due to this presynaptic change, rather than to alterations in synaptic density.

Because synapsin levels, and likely mEPSC frequency, covary with vesicle number and release (31, 32), it is possible that differences between WT and KO hippocampal synapses are evident in the electron microscope (Fig. 4). Samples were prepared from 44- to 45-day-old WT and KO intact hippocampi; the number of vesicles in a cluster and the length of PSDs were analyzed from single-plane sections of stratum radiatum in CA1. KO presynaptic nerve terminals contain 10% more synaptic vesicles than WT terminals ($P = 0.04$) (Fig. 4*b*). In contrast, measurements of PSD length in hippocampus do not differ significantly between genotypes (Fig. 4*c*), suggesting that postsynaptic parameters are not drastically changed, consistent with hippocampal neurons *in vitro*. However, postsynaptic orga-

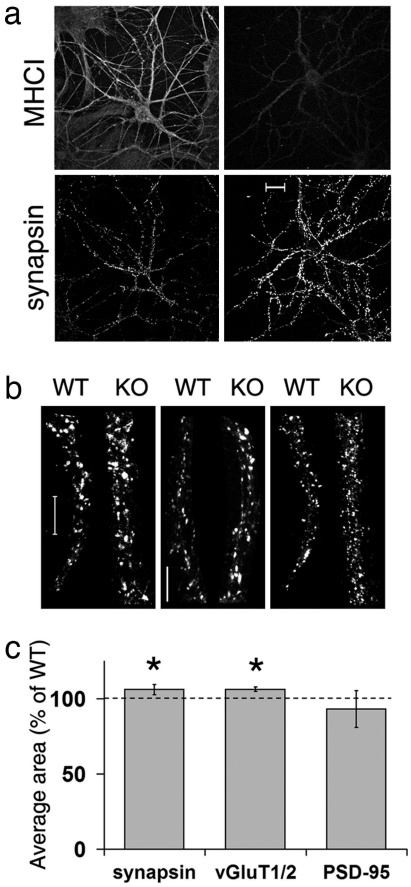

Fig. 3. Synaptic structure is altered in KO hippocampal neurons *in vitro*. (*a*) Intensity of MHCI immunostaining decreases in KO neurons (*Right*), whereas levels of synapsin increase compared with WT (2 weeks *in vitro*) (*Left*). (Scale bar: 20 μm.) (*b*) Synapsin (*Left*) and VGluT1/2 (*Center*) immunostained puncta appear larger in KO compared with WT; PSD-95 (*Right*) appears unchanged. (Scale bars: 10 μm.) (*c*) Quantification of synapsin, vGluT1/2, and PSD-95 immunoreactive puncta. Synapsin bouton size (average no. of pixels per bouton) is 6.2 $\pm$ 3.3% larger in KO relative to WT control ($P = 0.03$, $n = 6$ experiments). vGluT1/2 immunoreactive boutons in KO are 6.3 $\pm$ 1.6% larger than WT control ($P = 0.02$, $n = 3$ experiments). PSD-95 puncta size in KO is not significantly different from WT (93.2 $\pm$ 12.2; $P = 0.10$). Data represent mean $\pm$ SD. *, statistical significance by *t* test.

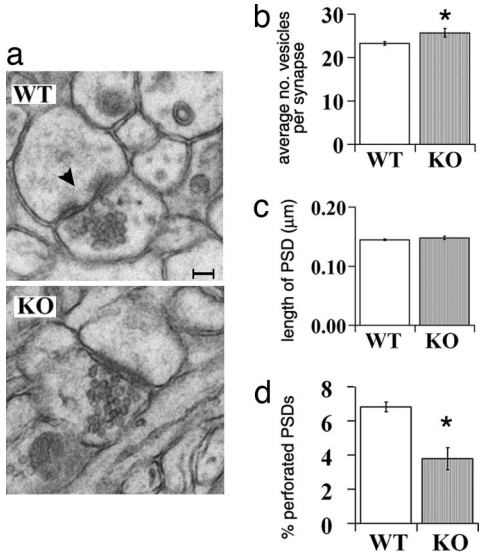

Fig. 4. Hippocampal synaptic ultrastructure is altered in KO mice. (*a*) Representative EM sections from WT and KO hippocampus. Black arrowhead, example of a perforated synaptic contact. (Scale bar: 50 nm.) (*b*) Increase in vesicle number in KO vs. WT synapses (WT, 23.3 $\pm$ 0.4; KO, 25.7 $\pm$ 1.0; $P = 0.04$). Data represent average of mean vesicle number per synaptic plane for three animals of each genotype $\pm$ SEM. A total of 522 WT synapses and 563 KO synapses were counted. (*c*) Postsynaptic densities (PSD) are not significantly longer in KO than WT (in μm) (WT, 0.145 $\pm$ 0.001; KO, 0.148 $\pm$ 0.003; $P = 0.19$). (*d*) Fewer perforations at KO hippocampal synapses than WT (3.8 $\pm$ 0.6% average perforated per total synapses per animal) compared with WT (6.8 $\pm$ 0.3%) ($P = 0.006$).

nization at KO hippocampal synapses is not entirely normal: The percent perforated PSDs is reduced in KO to about half the number in WT ($P = 0.006$) (Fig. 4*d*). Together these observations demonstrate that the synaptic changes in β2m/TAP1 mutant mice are both structural and functional.

Neuronal MHCI was discovered in a screen for genes regulated by blockade of neural activity with Tetrodotoxin (TTX) *in vivo* (7). In hippocampal cultures, TTX treatment is known to increase both mEPSC amplitude and frequency (38, 39). Furthermore, β2m/TAP1 KO mice have abnormal retinogeniculate projections, reminiscent of animals that have undergone chronic activity blockade (1, 20); these mice also have altered hippocampal synaptic plasticity (19). Together these findings suggest that MHCI may regulate a neuron's response to changes in levels of activity. To test this hypothesis, hippocampal cultures of both genotypes were grown in 1 μM TTX for 3–6 days and mEPSCs were recorded. Consistent with other reports, TTX treatment increased both mEPSC amplitude and frequency in WT hippocampal cultures. Median mEPSC frequency recorded from WT neurons treated with TTX increases 22% over WT neurons in vehicle, from 1.8–2.2 Hz. Median mEPSC amplitude increases more modestly from 7.0 pA in vehicle to 7.8 pA in TTX (Fig. 5 *a* and *b*). However, mEPSCs recorded from KO neurons grown in TTX do not increase significantly either instantaneous frequency or amplitude compared with KO neurons in vehicle (Fig. 5 *a* and *b*). This failure to regulate synaptic function in response to TTX blockade is not due to a problem with spiking activity in the KO cultures: Spontaneous spiking activity recorded with cell-attached patch is indistinguishable from WT cultures (Fig. 5*c*; SI Fig. 7).

Chronic TTX blockade regulates synaptic protein levels and vesicle release in cultured neurons (39–41). Consistent with the physiological observations above and previous reports, WT boutons immunostained for synapsin following TTX were 15 $\pm$ 5.0% larger than in vehicle control (SI Fig. 8 *a* and b). In these WT cultures, the size of PSD-95 immunoreactive puncta also increased (9.6 $\pm$ 5.8%) (SI Fig. 8*c*). This increase in PSD-95 puncta size correlates with reported increases in AMPA receptor levels following TTX treatment (30, 36, 37, 42). Unlike the increase in WT neurons following TTX treatment, PSD-95 puncta size in KO neurons does not increase (SI Fig. 8). No detectable change in synapse density was observed in either genotype following TTX treatment (data not shown). Thus, action potential activity blockade in WT cultures produces the expected changes in both pre- and postsynaptic morphological parameters, but the changes are more modest than reported previously. We attribute this difference to the automated measurements performed here by using stringent thresholding criteria (see *SI Methods*). Our observations also imply that KO synapses are unable to regulate synaptic structure in response to TTX: Presynaptic boutons are already enlarged and do not increase further with TTX, whereas postsynaptic properties such as PSD-95 puncta fail to adjust at all.

Together, the morphological and physiological abnormalities of KO neurons are reminiscent of synaptic changes following

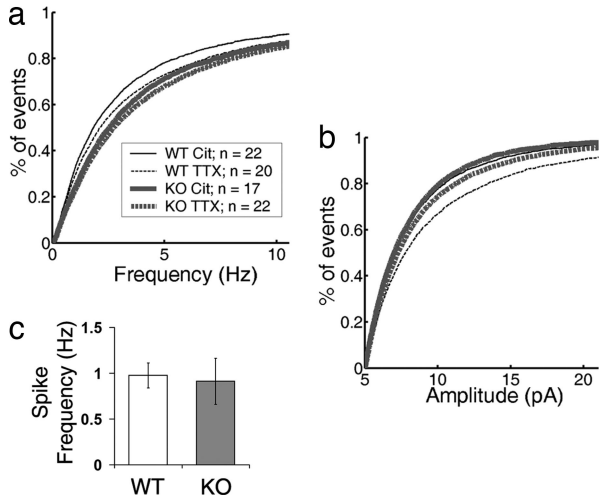

Fig. 5. mEPSCs fail to scale up with activity blockade in KO neurons. Fourteen-days *in vitro* WT and KO cultures were grown for 3–6 additional days in either 1 μM TTX or citrate control and then mEPSCs were recorded. (*a*) Cumulative distribution of instantaneous frequencies recorded from WT or KO cultures. In WT, TTX treatment increases mEPSC frequency compared with citrate control (control, 1.8 Hz; $n = 22$; TTX treated, 2.2 Hz; $n = 20$; $P = 0.09$). In KO, mEPSC frequency following TTX treatment is not significantly different ($P = 0.55$) from KO control (control, 2.5 Hz; $n = 17$; TTX treated, 2.7 Hz, $n = 22$ neurons). (*b*) Cumulative distribution of mEPSC amplitudes recorded from neurons in WT or KO cultures. In WT, TTX treatment increases mEPSC amplitude compared with control (control, 7.0 pA; TTX treated, 7.8 pA; $P < 0.001$). In KO, TTX treatment does not increase mEPSC amplitude (7.2 pA) over either WT or KO (7.0 pA) controls ($P = 0.62$). (*c*) Action potential activity is normal in cultures of KO hippocampal neurons as assessed by cell-attached patch recordings. Average spike frequency in WT, 0.97 Hz $\pm$ 0.14 ($n = 15$ neurons); KO, 0.91 Hz $\pm$ 0.25 ($n = 13$ neurons).

homeostatic synaptic plasticity or "synaptic scaling" (43, 44). Presynaptic bouton size and mEPSC frequency scale up following chronic activity blockade with TTX (38, 40, 45), reaching values similar to untreated cultures of β2m/TAP1 KO neurons. Moreover, MHCI was discovered in a differential display screen for genes regulated by TTX (7), suggesting it may contribute to the homeostatic response to changes in neuronal activity. If so, then treating WT hippocampal neurons with TTX should downregulate MHCI protein levels. Indeed, levels of MHCI immunoreactivity in WT cultures treated with TTX decreased to 31% of vehicle-treated cultures (SI Fig. 9). Thus, the increase in bouton size in WT hippocampal cultures grown in TTX is correlated with a decrease in neuronal MHCI protein. These observations suggest a function for MHCI as a key regulator of the presynaptic nerve terminal's response to sustained changes in neural activity.

Discussion

A major finding of this study is that MHCI is part of the molecular machinery regulating synaptic morphology and function under basal conditions and following action potential blockade. Four independent methods, whole-cell recordings and immunohistochemistry from hippocampal neurons *in vitro*, whole-cell recordings from cortical neurons in slices, and EM in intact hippocampus, have been used to demonstrate that synaptic structure and function are altered in β2m/TAP1 mutant mice lacking stable cell surface expression of MHCI. The functional changes assessed with physiology (e.g., increased mEPSC frequency) are more robust than the observed alterations in presynaptic morphology (e.g., size of immunostained boutons, EM vesicle numbers), but both are well correlated and support a role for MHCI in the control of synaptic function. Although we cannot rule out that the mEPSC frequency increase is due to an increase in the number of silent synapses (39, 46), we did not observe changes in synaptic density as estimated by immunostaining for PSD-95 or synapsin. Note also that the synaptic defects in KOs observed here are not in the initial assembly and function of synapses. Although synaptic function is altered, it is modest and not pathological, and action potential generation within these cultures, as well as in the intact animal (19), is within a normal range.

MHCI protein is detected at postsynaptic membranes of WT neurons, but presynaptic abnormalities are observed at KO synapses in the basal state, implying that MHCI may function as part of a retrograde signaling system. At present, it is not known whether this retrograde effect is direct, via transsynaptic signaling with a presynaptic MHCI receptor such as PIRB (23) that might modulate synaptic vesicle dynamics, or instead whether it is indirect, via interactions with postsynaptic components such as glutamate receptors. Because both MHCI mRNA and postsynaptically localized proteins are regulated by neural activity, MHCI could link presynaptic function with postsynaptic activity. It should be noted that normally pre- and postsynaptic elements are coregulated (30). However, in KO mice, there appears to be a mismatch: Presynaptic boutons, but not PSD-95 puncta, are enlarged in the basal state (and neither pre- nor postsynaptic elements respond normally to activity blockade). Our study suggests that MHCI may function to coordinate communication across the two sides of the synapse.

There is evidently also a problem in the homeostatic adjustment of synapses to match pre- with postsynaptic size in response to changes in neural activity within developing circuits in KO mice. Several experimental manipulations known to induce homeostatic synaptic scaling also increase both mEPSC frequency and the probability of release at excitatory synapses (12, 40, 47). Because the physiological relationship between spontaneous mEPSCs and evoked synaptic transmission is not entirely clear (48, 49), we cannot conclude with certainty that the changes in mEPSC frequency seen here indicate an increase in the probability of release at KO synapses. However, Murthy *et al.* (42) observed an increase in vesicle number following TTX treatment, consistent with our observed increase in synapsin immunoreactivity. The increases in synapsin and vGluT immunoreactivity also correlate with the increase in vesicle number observed in our EM analysis of intact KO hippocampus. Although the increase in vesicle number is modest ($\approx$10%), it is similar in magnitude to the changes observed here in synapsin and vGluT immunostaining. Note also that the EM analysis is likely to be an underestimate because synapses were assessed in single-plane images, only allowing 2D observation of the 3D vesicle pool. Serial section comparison of WT and KO neurons will be necessary to obtain more accurate vesicle counts.

We report that MHCI is needed for homeostatic scaling of synapses in response to activity blockade *in vitro*. Because our focus was on glutamatergic synapses, we do not know whether MHCI is required for homeostatic adjustments at inhibitory synapses, which could involve different mechanisms (50), nor do we know which of the >70 MHCI family members might contribute. Other molecules with immune function, such as TNFα, are also involved in homeostatic scaling at excitatory synapses (51). TNFα is known to regulate MHCI levels in hippocampal neurons *in vitro* (25) and thus may act via an MHCI-dependent pathway. Here we also show that MHCI protein levels are regulated by TTX. This finding is consistent with the decrease in MHCI mRNA observed after infusion of TTX into the developing brain (7) and with the increase in MHCI protein following glutamate receptor activation in cultured neurons (9). In the hippocampus, MHCI is downstream of the transcription factor CREB (8), suggesting that it is part of a molecular program for synapse scaling that also includes other

key members of a Ca^{2+}-regulated signaling pathway including CamKII and BDNF (12, 52, 53).

Although homeostatic scaling occurs in response to the amount of activity across the entire neuron, Hebbian mechanisms of LTP and LTD act to modulate strength at specific synapses. Models that explore changes in synaptic strength in a competitive, Hebbian manner generally need to invoke a "synaptic normalization," akin to synaptic scaling, to prevent uncontrolled positive feedback of potentiation and/or depression (44). Consequently, neuronal circuits unable to scale synaptic strength might also be expected to exhibit abnormalities in synaptic plasticity; this phenotype is observed in β2m/TAP1 mice, which have enhanced LTP and lack LTD (19). Together our observations reveal a dual role for MHCI in both forms of activity-dependent synaptic plasticity: MHCI, whose expression is modulated by overall levels of action potentials both *in vivo* (7) and *in vitro*, contributes to homeostatic plasticity, which in turn may set limits on the magnitude and direction of Hebbian synaptic plasticity.

Experimental Procedures

More details are found in *SI Methods*.

Hippocampal Cultures. All animals were treated in accordance with institutional guidelines. Cultures were derived from postnatal day 0 to postnatal day 1 mouse hippocampi by using standard protocol (54). Cultures were grown (2–3 weeks) on coverslips over a glial feeder layer in 12-well plates in 2 ml of Neurobasal media with B27 supplement (Invitrogen, Carlsbad, CA) and 3.7 μg/ml glutamate (Invitrogen), refreshing 1 ml of media without glutamate once after 4 days *in vitro* and again at 10 days to administer drug. Low-density cultures (Figs. 1 and 2*a*) were plated at 20,000 cells per 15-mm coverslip; high-density cultures were plated at 100,000 cells per coverslip (Figs. 3–5). KO mice were of the same genetic background as described (19). WT mice were of two types: derived from production of β2m/TAP1 KO (19) or from C57BL/6 from Charles River Breeding Laboratories (Portage, MI). When possible, WT and KO cultures were prepared on the same day; occasionally, WT and KO cultures were prepared 3–4 days apart. If derivation of cultures was separated by 1 day, cultures were treated and fixed simultaneously. For separations of >1 day, cultures were treated and fixed independently.

For activity manipulations, action potentials were blocked by adding 1 μM TTX (T5651; Sigma–Aldrich, St. Louis, MO; supplied in sodium citrate vehicle) to 13- or 14-days *in vitro* cultures; vehicle control was 5 μM sodium citrate (Sigma–Aldrich). One milliliter of culture media was removed and replaced with drug/vehicle to a final concentration of 1 μM for 5 days, refreshing on the third day.

Hippocampal Culture Physiology. High-density cultures (100,000 cells plated) were used after 14 days *in vitro*. [TTX treatments (3–6 days) began at day 13 or 14.] Whole-cell recordings were obtained at room temperature in standard artificial cerebrospinal fluid (in mM): 136 NaCl, 2.5 KCl, 10 glucose, 10 Hepes, 2 $CaCl_2$, 1.3 $MgCl_2$, containing 0.5 μM TTX, 20 μM bicuculline, and 50 μM AP5. Data were collected with an Axopatch 200B amplifier and pClamp 9.2. Pipets were pulled by using a Sutter P-97, with tip resistances of 4–9 MΩ. Internal solution contained (in mM): 130 potassium gluconate, 10 NaCl, 1 EGTA, 0.133 $CaCl_2$, 2 $MgCl_2$, 10 Hepes, 3.5 MgATP, and 1 NaGTP.

Cortical Slice Physiology. Coronal brain slices were cut (300-μm thick) from WT (derived from the generation of β2m/TAP1 KO mice) and β2m/TAP1 KO mice at P19–21 in ice-cold ACSF (in mM) 130 NaCl, 3 KCl, 1.25 NaH_2PO_4, 10 glucose, 20 $NaHCO_3$, 1.3 $MgSO_4$, and 2.5 $CaCl_2$) bubbled with 95% 0_2/5% CO_2. Slices were immediately transferred to 37°C ACSF bath for 30 min and then returned to room temperature. Recordings were performed at 31–32°C in oxygenated ACSF + 0.25 μM TTX, 25 μM APV, and 10 μM bicuculline. Pipets were pulled by using a Sutter P-97, with tip resistances of 4–8 MΩ. Internal solution consisted of (in mM) 115 CsMeSO4, 5 NaF, 10 EGTA, 10 Hepes, 15 CsCl, 3.5 MgATP, 3 QX-314, and Lucifer yellow. Slices were kept for up to 6 h.

MHCI Immunostaining. For all experiments, age-matched WT and KO cultures were immunostained and imaged together; imaging and analysis were done blind to genotype and treatment condition. Cultures were removed from media and immersed in paraformaldehyde (4% in PBS) at 37°C for 8 min. Anti-MHCI antibodies (Ox18, ERHR52) (7, 55) were added in 5% donkey serum (The Jackson Laboratory, Bar Harbor, ME) in PBS + 0.1% Tween (PBST) at 1 μg/ml. Sister cultures were immunostained with equimolar concentrations of isotype IgG as control (Ox18, Serotec, Oxford, U.K.; mouse IgG1, Sigma–Aldrich; M-5284, ERHR52, Bachem, Bubendorf, Switzerland; Peninsula Laboratories, Belmont, CA; Rat IgG2a, eBiosciences, San Diego, CA; 14–4321). Biotinylated donkey secondary antibody (The Jackson Laboratory) was added at 1/200 (anti-mouse) or 1/500 (anti-rat) for 1 h. Avidin-biotin amplification (Vector Laboratories, Burlingame, CA) was prepared in PBS and applied for 30 min. Cy3-conjugated tyramide (NEN Life Science Products, Boston, MA) was prepared in included diluent at 1/100 and added to cultures for 5 min. Then synapsin immunostaining was performed as described below by using rabbit anti-synapsin and goat anti-PSD-95 (for Ox18) or mouse anti-PSD-95 (for ERHR52).

Synaptic Marker Immunostaining. Primary and secondary antibodies were diluted in 5% donkey serum (The Jackson Laboratory) in PBST. Rabbit anti-synapsin (AB1543P; Chemicon International, Temecula, CA), 0.5 μg/ml; mouse anti-PSD-95 (MA1–045; Affinity Bioreagents, Golden, CO), 15 μg/ml; guinea pig anti-rat vGluT1 (AB5905; Chemicon) and vGluT2 (AB5907; Chemicon), 1/2000 (serum); and mouse anti-β-III-tubulin (MAB1637; Chemicon), 1 μl per culture (concentration not determined by manufacturer). Donkey Cy2 anti-rabbit and Cy3 anti-mouse (The Jackson Laboratory) were used at 1/300 dilutions. Cy5 Zenon reagent (Molecular Probes, Eugene, OR) was used to image tubulin; reagents were prepared following documentation from Molecular Probes. Cover slips were mounted onto slides with *N*-propyl-galate (Sigma–Aldrich) and sealed with DPX (Electron Microscopy Sciences, Hatfield, PA). Cultures were imaged on a LSM 510 (Carl Zeiss, Thornwood, NY) confocal microscopy system; 15–20 images were collected per cover slip. Images were taken at 1,024 × 1,024 resolution by using a Plan-Apochromat ×63/1.4 N.A. oil objective plus ×1.4 software zoom.

EM Methods. Age P44 β2m/TAP1 KO mice or WT mice ($n = 3$ each genotype; WT derived from generation of KO) were anesthetized with halothane and given a lethal injection of euthasol. Mice were perfused transcardially with normal 0.9% saline at 37°C, followed by at least 30 ml of 2.5% glutaraldehyde and 2% paraformaldehyde in 0.1 M sodium cacodylate buffer at 37°C. Brains were removed and postfixed overnight in the same fixative at 4°C; vibratome sections were cut (300-μm thick coronal) to expose hippocampus, and then blocks were cut from stratum radiatium. Blocks were treated with 1% osmium in potassium ferrocyanate and uranyl acetate. Thin sections (90 nm) were cut and placed on formvar grids. Grids were treated with uranyl acetate and Pb acetate. EM images were taken at ×10,000 magnification in stratum radiatum at a distance of 50–100 μm from stratum pyramidale.

We thank the Harvard Center for Neurodegeneration and Repair for access to the Confocal Microscopy Core facility. This work was supported by National Institutes of Health Grant R01 MH071666 and the Dana Foundation (to C.J.S.), a Goldenson Research Fellowship (to D.A.B.), and National Institutes of Health Grant T32 MH20017 and a Victoria and Stuart Quan fellowship (to C.A.G.).

1. Katz LC, Shatz CJ (1996) *Science* 274:1133–1138.
2. Lein ES, Hohn A, Shatz CJ (2000) *J Comp Neurol* 420:1–18.
3. Cabelli RJ, Shelton DL, Segal RA, Shatz CJ (1997) *Neuron* 19:63–76.
4. Lisman J, Schulman H, Cline H (2002) *Nat Rev Neurosci* 3:175–190.
5. Wong GH, Bartlett PF, Clark-Lewis I, Battye F, Schrader JW (1984) *Nature* 310:688–691.
6. Williams KA, Hart DN, Fabre JW, Morris PJ (1980) *Transplantation* 29:274–279.
7. Corriveau RA, Huh GS, Shatz CJ (1998) *Neuron* 21:505–520.
8. Barco A, Patterson S, Alarcon JM, Gromova P, Mata-Roig M, Morozov A, Kandel ER (2005) *Neuron* 48:123–137.
9. Kaltschmidt C, Kaltschmidt B, Baeuerle PA (1995) *Proc Natl Acad Sci USA* 92:9618–9622.
10. Ishii T, Hirota J, Mombaerts P (2003) *Curr Biol* 13:394–400.
11. Loconto J, Papes F, Chang E, Stowers L, Jones EP, Takada T, Kumanovics A, Fischer Lindahl K, Dulac C (2003) *Cell* 112:607–618.
12. Thiagarajan TC, Piedras-Renteria ES, Tsien RW (2002) *Neuron* 36:1103–1114.
13. Deisseroth K, Bito H, Schulman H, Tsien RW (1995) *Curr Biol* 5:1334–1338.
14. Fischer Lindahl K (1997) *Immunogenetics* 46:53–62.
15. Bijlmakers MJ, Ploegh HL (1993) *Curr Opin Immunol* 5:21–26.
16. Van Kaer L, Ashton-Rickardt PG, Ploegh HL, Tonegawa S (1992) *Cell* 71:1205–1214.
17. Zijlstra M, Bix M, Simister NE, Loring JM, Raulet DH, Jaenisch R (1990) *Nature* 344:742–746.
18. Neefjes JJ, Momburg F (1993) *Curr Opin Immunol* 5:27–34.
19. Huh GS, Boulanger LM, Du H, Riquelme PA, Brotz TM, Shatz CJ (2000) *Science* 290:2155–2159.
20. Upton AL, Salichon N, Lebrand C, Ravary A, Blakely R, Seif I, Gaspar P (1999) *J Neurosci* 19:7007–7024.
21. Godement P, Salaun J, Imbert M (1984) *J Comp Neurol* 230:552–575.
22. Stellwagen D, Shatz CJ (2002) *Neuron* 33:357–367.
23. Syken J, Grandpre T, Kanold PO, Shatz CJ (2006) *Science* 313:1795–1800.
24. Boulanger LM, Shatz CJ (2004) *Nat Rev Neurosci* 5:521–531.
25. Neumann H, Schmidt H, Cavalie A, Jenne D, Wekerle H (1997) *J Exp Med* 185:305–316.
26. Kennedy MB (1997) *Trends Neurosci* 20:264–268.
27. Greengard P, Browning MD, McGuinness TL, Llinas R (1987) *Adv Exp Med Biol* 221:135–153.
28. Zhong J, Zhang T, Bloch LM (2006) *BMC Neurosci* 7:17–29.
29. Linda H, Hammarberg H, Cullheim S, Levinovitz A, Khademi M, Olsson T (1998) *Exp Neurol* 150:282–295.
30. El-Husseini AE, Schnell E, Chetkovich DM, Nicoll RA, Bredt DS (2000) *Science* 290:1364–1368.
31. Hopf FW, Waters J, Mehta S, Smith SJ (2002) *J Neurosci* 22:775–781.
32. Pieribone VA, Shupliakov O, Brodin L, Hilfiker-Rothenfluh S, Czernik AJ, Greengard P (1995) *Nature* 375:493–497.
33. Ploegh HL, Cannon LE, Strominger JL (1979) *Proc Natl Acad Sci USA* 76:2273–2277.
34. Fremeau RT, Jr, Kam K, Qureshi T, Johnson J, Copenhagen DR, Storm-Mathisen J, Chaudhry FA, Nicoll RA, Edwards RH (2004) *Science* 304:1815–1819.
35. Fremeau RT, Jr, Voglmaier S, Seal RP, Edwards RH (2004) *Trends Neurosci* 27:98–103.
36. Kim E, Sheng M (2004) *Nat Rev Neurosci* 5:771–781.
37. Nakagawa T, Futai K, Lashuel HA, Lo I, Okamoto K, Walz T, Hayashi Y, Sheng M (2004) *Neuron* 44:453–467.
38. Burrone J, O'Byrne M, Murthy VN (2002) *Nature* 420:414–418.
39. Nakayama K, Kiyosue K, Taguchi T (2005) *J Neurosci* 25:4040–4051.
40. Murthy VN, Schikorski T, Stevens CF, Zhu Y (2001) *Neuron* 32:673–682.
41. De Gois S, Schafer MK, Defamie N, Chen C, Ricci A, Weihe E, Varoqui H, Erickson JD (2005) *J Neurosci* 25:7121–7133.
42. Beattie EC, Stellwagen D, Morishita W, Bresnahan JC, Ha BK, Von Zastrow M, Beattie MS, Malenka RC (2002) *Science* 295:2282–2285.
43. Burrone J, Murthy VN (2003) *Curr Opin Neurobiol* 13:560–567.
44. Turrigiano GG (1999) *Trends Neurosci* 22:221–227.
45. Turrigiano GG, Leslie KR, Desai NS, Rutherford LC, Nelson SB (1998) *Nature* 391:892–896.
46. Malenka RC, Nicoll RA (1997) *Neuron* 19:473–476.
47. Wierenga CJ, Walsh MF, Turrigiano GG (2006) *J Neurophysiol* 96:2127–2133.
48. Miller GL, Knudsen EI (2001) *J Neurophysiol* 85:2184–2194.
49. Bacci A, Huguenard JR (2006) *Neuron* 49:119–130.
50. Hartman KN, Pal SK, Burrone J, Murthy VN (2006) *Nat Neurosci*.
51. Stellwagen D, Malenka RC (2006) *Nature* 440:1054–1059.
52. Tyler WJ, Pozzo-Miller LD (2001) *J Neurosci* 21:4249–4258.
53. Rutherford LC, Nelson SB, Turrigiano GG (1998) *Neuron* 21:521–530.
54. Banker G, Goslin K (1998) (MIT Press, Cambridge, MA).
55. Neumann H, Cavalie A, Jenne DE, Wekerle H (1995) *Science* 269:549–552.